

Discrete-time sliding mode control based on disturbance observer applied to current control of permanent magnet synchronous motor

Thieli Smidt Gabbi¹  | Hilton Abílio Gründling²  | Rodrigo Padilha Vieira² 

¹ Electrical Engineering Department, Federal University of Rio Grande do Sul, 103 Osvaldo Aranha Av, Porto Alegre, Brazil

² Power Electronics and Control Group, Federal University of Santa Maria, 1000 Roraima Av, Santa Maria, Brazil

Correspondence

Thieli Smidt Gabbi, Electrical Engineering Department, Federal University of Rio Grande do Sul, 103 Osvaldo Aranha Av, Porto Alegre, Brazil.
Email: thieligabbi@gmail.com

Abstract

This paper proposes a robust current control technique based on a discrete-time sliding mode controller and a disturbance observer for high-performance permanent magnet synchronous motor (PMSM) drives. This scheme is applied in the PMSM current control loops to enable the decoupling between the dq current axes, rejection of disturbances caused by mechanical load changes and robustness under parametric uncertainties. In order to ensure the discrete-time sliding mode properties, which make the system cross the sliding surface at each sampling period, the PMSM model is extended, including the digital implementation delay resulting from the discrete-time algorithm execution. The development of this method allows direct implementation in microcontrollers and digital signal processors. Stability and convergence analysis are developed in the discrete-time domain. Simulation and experimental results demonstrate the effectiveness and good performance of the proposed current control approach.

1 | INTRODUCTION

Permanent magnet synchronous motors have been widely used in industrial and commercial drives, such as electric vehicles, wind generators, and robot applications. In electric vehicles, for example, traction motors are the key component for propulsion and require high torque and power density, wide speed range, high efficiency, high reliability, low noise, and reasonable cost [1, 2]. These characteristics are common in PMSM, however, the performance of this motor depends on hardware and controller design.

Field oriented control (FOC) methods are usually employed to ensure high performance of the drive. This method results in a cascade control structure with two inner current control loops and an outer speed control loop. This structure decouples the torque and flux by using the rotor dq reference frame. Also, the model in the synchronous reference has a direct relationship with the torque and current, so the current control is equivalent to the torque control [3]. Then, the current controller design is an essential task to ensure the good performance of the overall drive. However, the PMSM presents a non-linear model with

coupling between the dq current axes, especially under transient responses, load torque and parametric variations. In addition, the PMSM current loops are subjected to parametric variations, such as stator resistance, stator inductance, permanent magnet flux linkage and back-electromotive force, as well as being coupled with each other and also being highly dependent on speed [4]. Different current control scheme designed to improve the performance of the PMSM drive can also be found in the literature [3, 5–12].

Sliding mode (SM) techniques have been successfully applied to observers and controllers for systems with disturbances and parametric uncertainties. When compared with other robust methods, the SM is computationally simple and provides noticeable robustness and invariance properties to matched uncertainties [13–17]. There are several studies aiming at the development of sliding mode methods in the discrete-time domain due to their characteristics and to the advances in microcontrollers and digital signal processors. It allows the rapid prototyping of commercial solutions with SM, such as [18–21]. The design of the controller in the discrete-time domain is relevant because that stability conditions and the gains obtained in the

This is an open access article under the terms of the [Creative Commons Attribution](https://creativecommons.org/licenses/by/4.0/) License, which permits use, distribution and reproduction in any medium, provided the original work is properly cited.

© 2021 The Authors. *IET Power Electronics* published by John Wiley & Sons Ltd on behalf of The Institution of Engineering and Technology

continuous-time domain are not directly applied to discrete-time domain. When the design is carried out in the wrong way, it can produce chattering and even instability [14]. The reaching law approach is a procedure commonly used to design sliding mode controllers in discrete-time domain [22–26]. In [25], a reaching law is developed in order to carry the switching function to the sliding surface in a finite time. Thus, when the sliding surface is reached, a zigzag motion around the surface is obtained [27, 28].

The control law and sliding surface design in the conventional SM control (SMC) is based on the plant model, resulting in a controller which is insensitive to matched uncertainties, but sensitive to mismatched uncertainties [29]. Due to the importance of mitigating mismatched uncertainties in practical control applications, new SMC techniques have been proposed. There are several approaches combined with other control and observation methods, such as: schemes using linear matrix inequalities (LMI), integral action, fixed switching period or modifications in sliding surface [30–34]. In [32, 33] and [34], the SMC is combined with another strategy. The sliding mode method is associated with a backstepping strategy in order to control a tank system with non-linear model uncertainties and is cross-coupled in [34]. In addition, a PI controller is used to reduce the steady-state error. In [32] and [33] a sliding mode controller is based on the disturbance observer (DOB) technique. In order to improve the DC–DC converter system performance with mismatched disturbances, the SMCDOB is applied to control the output voltage of a buck converter in [33]. In [32], the SMCDOB is applied to a MAGLEV suspension system. The new sliding surface is designed using the disturbance estimation so that the sliding motion along the sliding surface tends to the equilibrium point even under the presence of mismatched uncertainties.

Control techniques based on the DOB becomes a good approach to deal with the presence of disturbances and to improve closed-loop system robustness [29]. A DOB design is presented in [35]. There are two advantages to the DOB in comparison to the other robust control techniques. One of them is the possibility to use it with other existing control methods improving the system robustness. The second advantage is obtained because the DOB is designed to work in the presence of disturbances, however, when these disturbances are not present, the behaviour of the system is not affected [36]. This control method can be used in industrial applications, such as mechatronics, chemical and aerospace systems [5, 7, 37]. The sliding mode control based on the disturbance observer (SMC-DOB) can enhance the reference tracking. The SMCDOB provides a good option as a control algorithm because even under plant variations, the algorithm will adapt the observed disturbance to mitigate the coupling effect, parametric variations, load disturbance and unknown uncertainties in the controller, as well as reduce chattering and increase system bandwidth [32, 38–43].

In [32, 38, 39, 41] and [42] the SMCDOB algorithm is developed in the continuous-time domain, which could be not ideal for practical systems. The algorithm is applied to the position control of PMSMs using a control law with non-linear feedback composed in [41]. In [40] the discrete-time SMCDOB is applied

in the superheated steam temperature systems. The algorithm is based on linear feedback technique and average dwell-time method. In addition, the combination of techniques increases the robustness and minimises the chattering. An algorithm using the higher-order SM for uncertain linear time-invariant systems is proposed in [43]. A disturbance forecast technique is adopted to estimate the future disturbance terms. A mass-spring-damper system in different operating situations of industry is used for the experimental tests. However, in [40] and [43], the equivalent control approach is employed to obtain the control laws. The zigzag motion around the surface is not guaranteed when the equivalent control is used. Moreover, if the sampling time is small, a large control input is needed and this may be undesirable in practice [16].

In order to provide a solution to the current control problem of the PMSM, this paper proposes a discrete-time controller, which combines a sliding mode technique with a disturbance observer. Differently from previous studies in the literature, this technique includes a digital implementation delay in the problem formulation, which allows a suitable form to operate with digital signal processors and PWM voltage source inverters, improving the performance of the overall PMSM drive. This paper compares the behaviour of the system with and without the inclusion of the digital implementation delay in the problem formulation. Moreover, the switching functions are modified to enable the system to cross the sliding surface at each sampling period, such as proposed in [25], which is not achieved when the digital implementation delay is neglected. The stability analysis of the proposed discrete-time disturbance observer is performed by means of a Lyapunov approach. A graphical analysis is presented in order to demonstrate the impact of the gain choice in the system stability. The main contributions of this paper can be summarised as:

- (i) the design of a new extended disturbance observer in the discrete-time domain, which is characterised by the inclusion of the plant state estimation, resulting in an improved disturbance observer;
- (ii) the inclusion of the new extended disturbance observer in the sliding mode current control law in the discrete-time domain;
- (iii) the proposal and analysis of the system in the discrete-time domain with the inclusion of the digital implementation delay;

As a result of the mentioned contributions, it was possible to obtain a control strategy with a simple structure that can be applied in different non-linear plants with mismatched uncertainties. The inclusion of the observed disturbances in the sliding mode current control law mitigates the coupling effect in dq axes and improves the system robustness. In addition, the combination of SMC and DOB provides a reduction in the values of SMC gains, mitigating the chattering effect.

Simulation and experimental results are carried out to evaluate the performance of the proposed decoupled current control scheme. These results are compared with the PI controller, with and without a disturbance observer, and with the conventional SMC.

2 | DYNAMIC MODEL OF PMSM

To obtain the PMSM mathematical model, consider the following assumptions [1]:

1. Stator windings are balanced with sinusoidally distributed magnetomotive force.
2. Inductance versus rotor position is sinusoidal.
3. Saturation and parameter changes are neglected.

The PMSM can be expressed in a synchronous reference frame by the following continuous-time non-linear equation:

$$\frac{d}{dt} \mathbf{i}_{dq(t)} = \boldsymbol{\gamma}_{dq} \mathbf{i}_{dq(t)} + \boldsymbol{\varsigma}_{dq} \mathbf{v}_{dq(t)} + \mathbf{d}_{dq(t)}. \quad (1)$$

The vectors and matrices in (1) are defined by,

$$\begin{aligned} \mathbf{i}_{dq(t)} &\triangleq [i_d(t) \ i_q(t)]^T, \quad \mathbf{v}_{dq(t)} \triangleq [v_d(t) \ v_q(t)]^T, \\ \boldsymbol{\gamma}_{dq} &\triangleq \begin{bmatrix} -\frac{R_s}{L_d} & 0 \\ 0 & -\frac{R_s}{L_q} \end{bmatrix}, \quad \boldsymbol{\varsigma}_{dq} \triangleq \begin{bmatrix} \frac{1}{L_d} & 0 \\ 0 & \frac{1}{L_q} \end{bmatrix}, \\ \mathbf{d}_{dq(t)} &\triangleq \begin{bmatrix} 0 & \frac{P L_q}{L_d} \omega_r(t) \\ -\frac{P L_d}{L_q} \omega_r(t) & 0 \end{bmatrix} \mathbf{i}_{dq(t)} - \begin{bmatrix} 0 \\ \frac{P \phi_{srm}}{L_q} \omega_r(t) \end{bmatrix}, \end{aligned}$$

where R_s is the stator resistance, L_d is the inductance of d -axis, L_q is the inductance of q -axis, P is the number of pole pairs, ϕ_{srm} is the permanent magnet flux linkage, i_d and i_q are the stator currents referred to synchronous reference frame, v_d and v_q are the stator voltages in a synchronous reference frame and ω_r is the rotor speed.

For a sufficiently small sampling period T_s , Equation (1) can be discretised using the forward Euler method. In addition, the cross-coupling terms and parametric uncertainties of the model are included as disturbances (d_d and d_q), which results in the discretised model,

$$\mathbf{i}_{dq(k+1)} = (\mathbf{I} + T_s \boldsymbol{\gamma}_{dq}) \mathbf{i}_{dq(k)} + T_s \boldsymbol{\varsigma}_{dq} \mathbf{v}_{dq(k)} + T_s \mathbf{d}_{dq(k)}, \quad (2)$$

where, $\mathbf{i}_{dq(k)} \triangleq [i_d(k) \ i_q(k)]^T$, $\mathbf{v}_{dq(k)} \triangleq [v_d(k) \ v_q(k)]^T$.

The disturbances $\mathbf{d}_{dq(k)} \triangleq [d_d(k) \ d_q(k)]^T$ are defined as,

$$\begin{aligned} \mathbf{d}_{dq(k)} &\triangleq \begin{bmatrix} 0 & \frac{P L_q}{L_d} \omega_r(k) \\ -\frac{P L_d}{L_q} \omega_r(k) & 0 \end{bmatrix} \begin{bmatrix} i_d(k) \\ i_q(k) \end{bmatrix} + \\ &+ \begin{bmatrix} 0 \\ -\frac{P \phi_{srm}}{L_q} \omega_r(k) \end{bmatrix} + \begin{bmatrix} \zeta_d(k) \\ \zeta_q(k) \end{bmatrix}, \quad (3) \end{aligned}$$

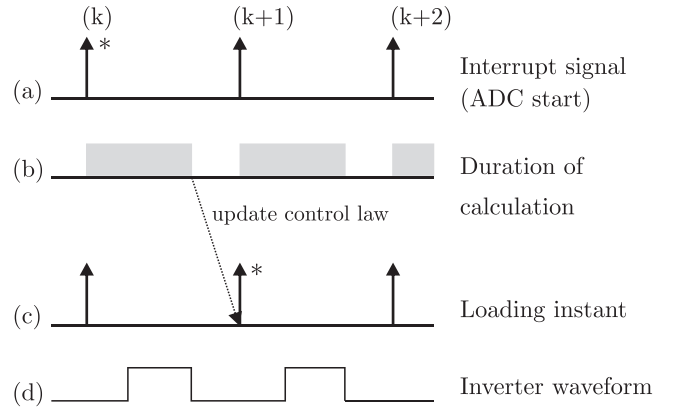


FIGURE 1 Sequence of digital implementation. (a) Interrupt signal generated by PWM; (b) duration of calculation; (c) loading the controller output; (d) application of the phase voltage on the inverter by PWM. (*) means the order of procedure.

where $\zeta_d(k)$ and $\zeta_q(k)$ represent parametric uncertainties and unmodelled dynamics. It is important to note that parametric changes of the model directly affect the terms $\zeta_d(k)$ and $\zeta_q(k)$. According to [1], the main parametric variations that affect the model are R_s and ϕ_{srm} due to temperature, and L_q when the motor operates in the saturation region. In addition, note that the cross-coupling is directly dependent on the rotor speed, in (3). Therefore, when the rotor speed is high, a change in one of the dq currents results in a torque distortion and in a high transitory disturbance in the other axis current.

New states ($\boldsymbol{\psi}_d$ and $\boldsymbol{\psi}_q$) are added in the discrete PMSM model aiming to include the effect of the digital implementation delay, which results in an extended model suitable for applications using microcontrollers and digital processors. The digital implementation is carried out in fixed time intervals or interruptions, as presented in Figure 1(a) in terms of samples (k), ($k+1$) and ($k+2$). The interruption is started synchronised with the k^* signal, when the AD converter samples the values of the phase currents, DC bus voltage and rotor position to calculate the output voltages. As an example, the grey period shown in Figure 1(b) illustrates the time required for the control law calculation. This control law is only applied in the next time sampling, as shown in Figure 1(c). During the period of ($k+1$), the phase voltages calculated in period k are applied to the motor by means of the inverter, as shown in Figure 1(d). One sample delay in the system model is the result of the process depicted by Figure 1.

The resulting extended model is given by,

$$\mathbf{i}_{dq(k+1)} = \boldsymbol{\Gamma}_{dq} \mathbf{i}_{dq(k)} + T_s \boldsymbol{\varsigma}_{dq} \boldsymbol{\psi}_{dq(k)} + T_s \mathbf{d}_{dq(k)}, \quad (4)$$

$$\boldsymbol{\psi}_{dq(k+1)} = \begin{bmatrix} \boldsymbol{\psi}_d(k+1) \\ \boldsymbol{\psi}_q(k+1) \end{bmatrix} = \begin{bmatrix} v_d(k) \\ v_q(k) \end{bmatrix}. \quad (5)$$

where, $\boldsymbol{\Gamma}_{dq} = (\mathbf{I} + T_s \boldsymbol{\gamma}_{dq})$.

3 | DISCRETE-TIME SLIDING MODE BASED ON DISTURBANCE OBSERVER CONTROLLER

3.1 | Discrete-time disturbance observer

This paper proposes a new discrete-time disturbance observer, which is combined with a sliding mode controller. This algorithm uses the estimation of the dq currents and an additional state to compute the expression of the observed disturbance, as given by

$$\begin{cases} \mathbf{p}_{dq(k+1)} = \mathbf{p}_{dq(k)} - T_s \left(-l_1 \boldsymbol{\gamma}_{dq} \mathbf{i}_{dq(k)} + l_1 \boldsymbol{\varsigma}_{dq} \mathbf{v}_{dq(k)} + \right. \\ \quad \left. + l_1 \mathbf{p}_{dq(k)} + l_1^2 \mathbf{i}_{dq(k)} - (l_1 - l_2) \tilde{\mathbf{i}}_{dq(k)} \right) \\ \hat{\mathbf{d}}_{dq(k)} = \mathbf{p}_{dq(k)} + l_1 \mathbf{i}_{dq(k)} - l_2 \tilde{\mathbf{i}}_{dq(k)} \\ \hat{\mathbf{i}}_{dq(k+1)} = \hat{\mathbf{i}}_{dq(k)} + T_s \left(-\boldsymbol{\gamma}_{dq} \mathbf{i}_{dq(k)} + \boldsymbol{\varsigma}_{dq} \mathbf{v}_{dq(k)} + \hat{\mathbf{d}}_{dq(k)} + \right. \\ \quad \left. - l_2 \tilde{\mathbf{i}}_{dq(k)} \right), \end{cases} \quad (6)$$

where, $\mathbf{p}_{dq(k)} = [p_{d(k)} \ p_{q(k)}]^T$ is the state vector of the observer, $\hat{\mathbf{d}}_{dq(k)} = [\hat{d}_{d(k)} \ \hat{d}_{q(k)}]^T$ the observed disturbance vector, $\hat{\mathbf{i}}_{dq(k)} = [\hat{i}_{d(k)} \ \hat{i}_{q(k)}]^T$ the observed currents vector, $\tilde{\mathbf{i}}_{dq(k)} = [\tilde{i}_{d(k)} \ \tilde{i}_{q(k)}]^T$ the current estimation vector error, l_1 and l_2 are positive gains.

The current estimation errors are defined as,

$$\tilde{\mathbf{i}}_{dq(k+1)} \triangleq \hat{\mathbf{i}}_{dq(k+1)} - \mathbf{i}_{dq(k+1)}. \quad (7)$$

The disturbance estimation errors are given by,

$$\tilde{\mathbf{d}}_{dq(k+1)} \triangleq \hat{\mathbf{d}}_{dq(k+1)} - \mathbf{d}_{dq(k+1)}. \quad (8)$$

3.2 | Stability analysis of discrete-time disturbance observer

Theorem 1 is presented to carry out the disturbance observer stability analysis.

Theorem 1. Consider the discretised system given by (2) and (3), subject to,

Assumption 1 (A1): The disturbance $d_{dq(k)}$ in the system (2) is bounded, that is $|d_{dq(k)}| \leq d_{dq}^*$, where d_{dq}^* is the upper bound of the disturbance.

Assumption 2 (A2): The discrete variation of the disturbance over one sampling period, $\Delta d_{dq(k)} = d_{dq(k+1)} - d_{dq(k)}$, is bounded and $\Delta d_{dq(k)} \rightarrow 0$ when $k \rightarrow \infty$. Then the discrete-time disturbance observer in (6) is stable and $\tilde{\mathbf{i}}_{dq(k)}$ and $\tilde{\mathbf{d}}_{dq(k)}$ goes to zero when $k \rightarrow \infty$.

Proof. The stability analysis of the disturbance observer proposed in (6) can be performed by means of the Lyapunov approach. Here, this analysis is exemplified for the d -axis. Note

that a similar analysis could be conducted for the q -axis, since the coupling and rotor speed dependent terms are modelled as disturbances. Thus, consider the following Lyapunov candidate function,

$$V_{(k)} = \tilde{d}_{d(k)}^2 + \tilde{i}_{d(k)}^2. \quad (9)$$

The difference equation of the current error expression can be obtained by replacing (2) and (6) in (7), which results,

$$\tilde{i}_{d(k+1)} = (1 - T_s l_2) \tilde{i}_{d(k)} + T_s \tilde{d}_{d(k)}. \quad (10)$$

The expression of the disturbance observer error is obtained replacing (2) and (6) in (8), such that,

$$\tilde{d}_{d(k+1)} = (1 - l_1 T_s - l_2 T_s) \tilde{d}_{d(k)} - \Delta d_{d(k)}. \quad (11)$$

From Assumption A2, $\Delta d_{d(k)} \rightarrow 0$ when $k \rightarrow \infty$, then, it is possible to rewrite (11) as,

$$\tilde{d}_{d(k+1)} = (1 - l_1 T_s - l_2 T_s) \tilde{d}_{d(k)}. \quad (12)$$

The difference equation of (9) is,

$$\begin{aligned} \Delta V_{(k)} &= V_{(k+1)} - V_{(k)}, \\ \Delta V_{(k)} &= \tilde{d}_{d(k+1)}^2 - \tilde{d}_{d(k)}^2 + \tilde{i}_{d(k+1)}^2 - \tilde{i}_{d(k)}^2. \end{aligned} \quad (13)$$

Solving (13) from (10) and (12), results,

$$\begin{aligned} \Delta V_{(k)} &= ((1 - l_1 T_s - l_2 T_s) \tilde{d}_{d(k)})^2 - \tilde{d}_{d(k)}^2 + \\ &+ ((1 - T_s l_2) \tilde{i}_{d(k)} + T_s \tilde{d}_{d(k)})^2 - \tilde{i}_{d(k)}^2. \end{aligned} \quad (14)$$

Rewriting (14),

$$\Delta V_{(k)} = -a \tilde{d}_{d(k)}^2 - b \tilde{i}_{d(k)}^2 - c (\tilde{d}_{d(k)} - \tilde{i}_{d(k)})^2, \quad (15)$$

where, $a = (1 - c_1^2 - T_s + c_2 T_s)$, $b = (1 - c_2^2 + c_2 T_s)$, $c = c_2 T_s$. The c_1 and c_2 are defined by, $c_1 = (1 - l_1 T_s - l_2 T_s)$ and $c_2 = (1 - T_s l_2)$. For the appropriate design of l_1 and l_2 , that ensures a, b and c positive, the expression (15) will be negative defined, which will make $V_{(k)} = 0$ when $k \rightarrow \infty$. \square

Remark 1: Assumption A2 is not very restrictive in electric machines systems. The disturbance expressions given in (3) are dependent of the stator currents, rotor speed, model parameters and parametric uncertainties. The stator currents are in a synchronous reference frame with DC characteristic and these currents are constant in steady state operation (constant rotor speed and constant load). In addition, the rotor speed dynamic is slower than the electrical dynamics, therefore, for small values of T_s it can be assumed constant. If a fast change is imposed to the stator current, the disturbance will change in

accordance with this current, however, the disturbance variation Δd_{qd} will assume a limited value. Moreover, in steady-state the disturbance will vary slowly in agreement with the rotor speed dynamic.

3.3 | Current control by the conventional sliding mode approach

Generally, the first step in the design of a discrete-time controller is the choice of the reaching control laws. The literature presents two groups of reaching laws for the discrete-time sliding mode approach: based on inequalities [22–24] and based on equalities [25, 26, 44]. This paper adopts the reaching law proposed by [25], where the control law can be obtained from the equality given by,

$$s_{n(k+1)} - s_{n(k)} = -qT_s s_{n(k)} - \epsilon T_s \text{sign}(s_{n(k)}), \quad (16)$$

where s_n is the sliding surface, the subscript n represents the direct or quadrature dq axes, ϵ and q are positive gains and $1 - qT_s > 0$, $\epsilon > 0$ and $q > 0$.

The reaching law given by (16) defines a quasi-sliding mode band, in which the trajectory of the discrete variable structure system crosses the sliding surface every sampling period, resulting in a zigzag motion.

Conventional sliding mode approach defines the switching function as an error between a measured value and its reference, for example $s_{n(k)} = i_{n(k)} - i_{n(k)}^*$. Note that this choice implies the knowledge of the future reference ($i_{n(k+1)}^*$) to obtain the expression of $s_{n(k+1)}$ given in (16). In order to avoid this problem, the current reference was delayed in one sampling period, such that,

$$s_{dq(k)} = \mathbf{i}_{dq(k)} - \mathbf{i}_{dq(k-1)}^*, \quad (17)$$

where the vectors $\mathbf{s}_{dq(k)}$ and $\mathbf{i}_{dq(k)}^*$ are defined as,

$$\mathbf{s}_{dq(k)} \triangleq [s_{d(k)} \ s_{q(k)}]^T, \quad \mathbf{i}_{dq(k)}^* \triangleq [i_{d(k)}^* \ i_{q(k)}^*]^T. \quad (18)$$

Thus, $s_{dq(k+1)}$ can be obtained from (2), as follows,

$$\begin{aligned} s_{dq(k+1)} &= \mathbf{i}_{dq(k+1)} - \mathbf{i}_{dq(k)}^* \\ &= \mathbf{\Gamma}_{dq} \mathbf{i}_{dq(k)} + T_s \mathbf{\zeta}_{dq} \mathbf{v}_{dq(k)} + T_s \mathbf{d}_{dq(k)} - \mathbf{i}_{dq(k)}^*. \end{aligned} \quad (19)$$

The control law can be obtained by replacing the expressions (17) and (19) in (16), which results,

$$\begin{aligned} \mathbf{v}_{dq(k)} &= \left(T_s \mathbf{\zeta}_{dq} \right)^{-1} \left[(\mathbf{I} - \mathbf{\Gamma}_{dq}) \mathbf{i}_{dq(k)} - T_s \mathbf{d}_{dq(k)} + \mathbf{i}_{dq(k)}^* + \right. \\ &\quad \left. - \mathbf{i}_{dq(k-1)}^* - qT_s \mathbf{s}_{dq(k)} - \epsilon T_s \text{sign}(\mathbf{s}_{dq(k)}) \right]. \end{aligned} \quad (20)$$

Then, replacing the actual disturbances, $\mathbf{d}_{dq(k)}$, by its observed values, $\hat{\mathbf{d}}_{dq(k)}$, the control law $\mathbf{v}_{dq(k)}$ is written in the form,

$$\begin{aligned} \mathbf{v}_{dq(k)} &= \left(T_s \mathbf{\zeta}_{dq} \right)^{-1} \left[(\mathbf{I} - \mathbf{\Gamma}_{dq}) \mathbf{i}_{dq(k)} - T_s \hat{\mathbf{d}}_{dq(k)} + \mathbf{i}_{dq(k)}^* + \right. \\ &\quad \left. - \mathbf{i}_{dq(k-1)}^* - qT_s \mathbf{s}_{dq(k)} - \epsilon T_s \text{sign}(\mathbf{s}_{dq(k)}) \right]. \end{aligned} \quad (21)$$

When the control law is implemented in digital signal processors, such as presented in Figure 1, the control law calculated in the sample (k) is only updated in the next sample ($k+1$). In other words, the control law used in sample (k) was calculated in sample ($k-1$). Thus, the dynamic of the PMSM can be obtained by replacing (21) in (4), which results,

$$\begin{aligned} \mathbf{i}_{dq(k+1)} &= \mathbf{\Gamma}_{dq} (\mathbf{i}_{dq(k)} - \mathbf{i}_{dq(k-1)}) - T_s \hat{\mathbf{d}}_{dq(k-1)} + \mathbf{i}_{dq(k-1)}^* + \\ &\quad (1 - qT_s) \mathbf{s}_{dq(k-1)} - \epsilon T_s \text{sign}(\mathbf{s}_{dq(k-1)}). \end{aligned} \quad (22)$$

From the analysis of (22) it is possible to observe that the choice of switching function (17) is not suitable to obtain the zigzag motion proposed by the reaching control law (16). Therefore, it is necessary to develop a new switching function taking into account the model with the inclusion of the digital implementation delay.

3.4 | Design of the discrete-time sliding mode controller based disturbance observer

Due to the presence of the digital implementation delay in the extended model, the switching function must be changed aiming to obtain a control law from (16). The new switching functions are based on sample ($k+1$) of the dynamic model. The current reference is delayed to allow the control law to be written with past values of the reference (see (24)). The resulting switching functions are given by,

$$\begin{aligned} \mathbf{s}_{dq(k)} &= \mathbf{i}_{dq(k+1)} - \mathbf{i}_{dq(k-1)}^* \\ &= \mathbf{\Gamma}_{dq} \mathbf{i}_{dq(k)} + T_s \mathbf{\zeta}_{dq} \mathbf{\psi}_{dq(k)} + T_s \mathbf{d}_{dq(k)} - \mathbf{i}_{dq(k-1)}^*. \end{aligned} \quad (23)$$

Note that expression (23) is developed based on the actual disturbances. These values are replaced by their observed values in implementation. The step ($k+1$) of the switching function is obtained to make possible to calculate (16), as follows,

$$\begin{aligned} \mathbf{s}_{dq(k+1)} &= \mathbf{i}_{dq(k+2)} - \mathbf{i}_{dq(k)}^* \\ &= \mathbf{\Gamma}_{dq} \left(\mathbf{\Gamma}_{dq} \mathbf{i}_{dq(k)} + T_s \mathbf{\zeta}_{dq} \mathbf{\psi}_{dq(k)} + T_s \mathbf{d}_{dq(k)} \right) + \\ &\quad + T_s \mathbf{\zeta}_{dq} \mathbf{\psi}_{dq(k+1)} + T_s \mathbf{d}_{dq(k+1)} - \mathbf{i}_{dq(k)}^*. \end{aligned} \quad (24)$$

The system will track the reference with two delays ($2T_s$) as consequence of the choice of switching functions in (23) and

(24). This can be verified by means of convergence analysis (see (29)). For small values of T_s , the system can operate with this delay.

The control law is obtained from (16). Replacing (23) and (24) in (16) it is possible to obtain the dq -axes control law, which is given by

$$\begin{aligned} v_{dq(k)} = & \left(T_s \boldsymbol{\varsigma}_{dq}\right)^{-1} \left[(\mathbf{I} - \boldsymbol{\Gamma}_{dq}) \left(\boldsymbol{\Gamma}_{dq} \mathbf{i}_{dq(k)} + T_s \boldsymbol{\varsigma}_{dq} \boldsymbol{\psi}_{dq(k)} + \right. \right. \\ & \left. \left. + T_s \mathbf{d}_{dq(k)} \right) - T_s \mathbf{d}_{dq(k+1)} + \mathbf{i}_{dq(k)}^* - \mathbf{i}_{dq(k-1)}^* + \right. \\ & \left. - q T_s \mathbf{s}_{dq(k)} - \epsilon \text{sign}(\mathbf{s}_{dq(k)}) \right]. \end{aligned} \quad (25)$$

Expression (25) presents variables dependent on the disturbance that are not computable. Then, using Assumption A2 and replacing the actual disturbances, $\mathbf{d}_{dq(k)}$, by their observed values, $\hat{\mathbf{d}}_{dq(k)}$, the discrete-time sliding mode control law combined with the observed disturbance is obtained, such that,

$$\begin{aligned} v_{dq(k)} = & \boldsymbol{\psi}_{dq(k+1)} \\ = & \left(T_s \boldsymbol{\varsigma}_{dq}\right)^{-1} \left[(\mathbf{I} - \boldsymbol{\Gamma}_{dq}) \left(\boldsymbol{\Gamma}_{dq} \mathbf{i}_{dq(k)} + T_s \boldsymbol{\varsigma}_{dq} \boldsymbol{\psi}_{dq(k)} \right) + \right. \\ & \left. - \boldsymbol{\Gamma}_{dq} T_s \hat{\mathbf{d}}_{dq(k)} + \mathbf{i}_{dq(k)}^* - \mathbf{i}_{dq(k-1)}^* - q T_s \mathbf{s}_{dq(k)} + \right. \\ & \left. - \epsilon \text{sign}(\mathbf{s}_{dq(k)}) \right]. \end{aligned} \quad (26)$$

3.5 | Convergence analysis of the PMSM with the discrete-time sliding mode current controller and disturbance observer

From the control law defined in (26), step $(k-1)$ can be written as,

$$\begin{aligned} v_{dq(k-1)} = & \boldsymbol{\psi}_{dq(k)} \\ v_{dq(k-1)} = & \left[(\mathbf{I} - \boldsymbol{\Gamma}_{dq}) \left(\boldsymbol{\Gamma}_{dq} \mathbf{i}_{dq(k-1)} + T_s \boldsymbol{\varsigma}_{dq} \boldsymbol{\psi}_{dq(k-1)} \right) + \right. \\ & \left. + T_s \boldsymbol{\Gamma}_{dq} \hat{\mathbf{d}}_{dq(k-1)} + \mathbf{i}_{dq(k-1)}^* - \mathbf{i}_{dq(k-2)}^* + \right. \\ & \left. - q T_s \mathbf{s}_{dq(k-1)} - \epsilon T_s \text{sign}(\mathbf{s}_{dq(k-1)}) \right] \left(T_s \boldsymbol{\varsigma}_{dq} \right)^{-1}. \end{aligned} \quad (27)$$

The dynamic of the PMSM with the proposed controller can be obtained by replacing the control law (27) in (4), which results,

$$\begin{aligned} \mathbf{i}_{dq(k+1)} = & (1 - q T_s) \mathbf{s}_{dq(k-1)} - \epsilon T_s \text{sign}(\mathbf{s}_{dq(k-1)}) + \\ & + \mathbf{i}_{dq(k-1)}^* + T_s \boldsymbol{\Gamma}_{dq} \hat{\mathbf{d}}_{dq(k)}. \end{aligned} \quad (28)$$

Note that the dynamics of the PMSM currents with the proposed controller, in accordance with (28), are dependent on the discrete-time SMC function, the switching functions, the

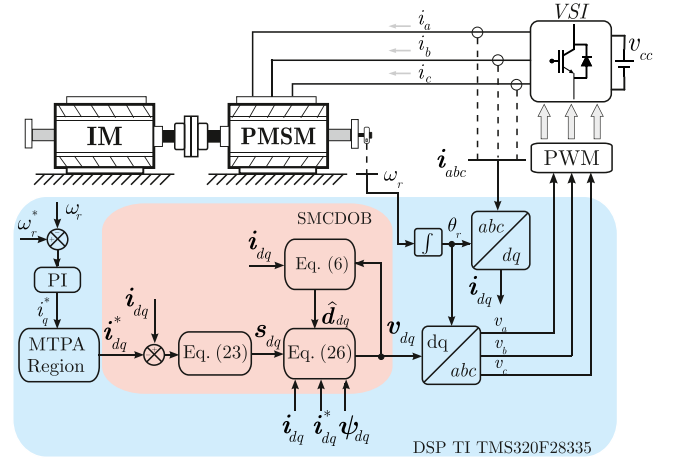


FIGURE 2 Block diagram of the proposed control scheme

delayed references and the disturbance observer error. Thus, the composite system of the switching functions and disturbance observer errors is presented as follows,

$$\begin{cases} \mathbf{s}_{dq(k)} = (1 - q T_s) \mathbf{s}_{dq(k-1)} - \epsilon T_s \text{sign}(\mathbf{s}_{dq(k-1)}) + \\ \quad + T_s \boldsymbol{\Gamma}_{dq} \hat{\mathbf{d}}_{dq(k)} \\ \hat{\mathbf{d}}_{dq(k+1)} = (1 - T_s l_1 - T_s l_2) \hat{\mathbf{d}}_{dq(k)} - \Delta \mathbf{d}_{dq(k)}. \end{cases} \quad (29)$$

The expressions given by (29) present the tracking error and disturbance observer error dynamics. From Assumption A2, the disturbance observer errors converge to zero for appropriate values of l_1 and l_2 when $k \rightarrow \infty$ (see Section 3.2 and Figure 5). If $\Delta \mathbf{d}_{dq(k)}$ is different from zero, the practical value for these variables are very small in steady-state condition using high sampling frequency, thus, the maximum disturbance observer errors will be bounded to these small values. Moreover, once the system reaches the sliding surface, it will cross this sliding surface each sampling period. When a perturbation occurs in the system, it will converge to zero in accordance with $\mathbf{s}_{dq(k)} = (1 - q T_s) \mathbf{s}_{dq(k-1)}$, for $(1 - q T_s) > 0$, if the disturbance observer errors are close to zero.

4 | SIMULATION AND EXPERIMENTAL RESULTS

Simulations and experimental results are presented in order to demonstrate the effectiveness of the proposed current control approach. A DSP TI TMS320F28335 was used with a three-phase voltage source inverter (VSI) to carry out the experimental results. The geometric approach for PWM modulation was adopted, according to [45]. The switching frequency used was 10 kHz which is equivalent to a sampling period of 100 μ s.

The block diagram of the proposed control scheme is depicted in Figure 2. It is possible to note the simple

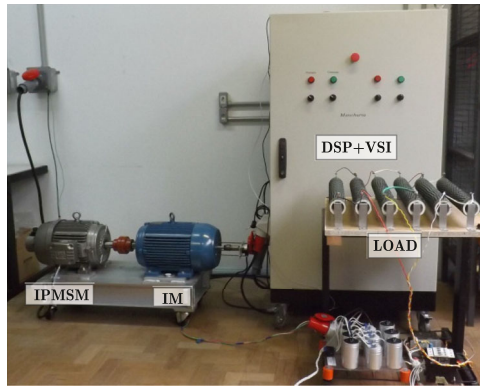


FIGURE 3 Experimental platform

TABLE 1 Electrical and Mechanical parameters of the PMSM

P_{rated}	11 kW
n_{rated}	1800 RPM
i_{rated}	19,29 A
R_s	0,5 Ω
L_d	20,1 mH
L_q	40,9 mH
J	0,03877 kgm ²
B	0,0194 Nms
ϕ_{srn}	0,5126 V/rad/s
P	3

implementation structure, which is carried out through expressions (6), (23) and (26).

Figure 3 presents a picture of the experimental platform. Table 1 presents the rated parameters of the PMSM. An induction machine (IM) is connected to the rotor shaft of the PMSM to provide mechanical load. The IM is used as a generator with a capacitor bank and a variable load, which allows to change the mechanical load applied in the PMSM rotor shaft.

In the first test, in both simulation and experimental, the rotor speed is not controlled. The rotor speed is kept in open loop while the currents i_d and i_q are controlled. Then, i_q^* is changed in order to observe the coupling between the axes. The second test, only experimental, the rotor speed loop is closed and the i_q^* is generated from the output of the PI controller of the rotor speed loop. The reference current i_d^* is calculated by (30) in the maximum torque-per-ampere region (below rated speed). This reference has been adapted from [46]. The rotor speed reference and currents references are the same in simulation and experimental tests to demonstrate the coupling between the dq axes and to evaluate the performance of the controller.

$$i_d^*(k) = \frac{\sqrt{3/2}\phi_{\text{srn}}}{2P(L_q - L_d)} - \sqrt{\frac{(\sqrt{3/2}\phi_{\text{srn}})^2}{4P^2(L_q - L_d)^2} + i_q^*(k)^2}. \quad (30)$$

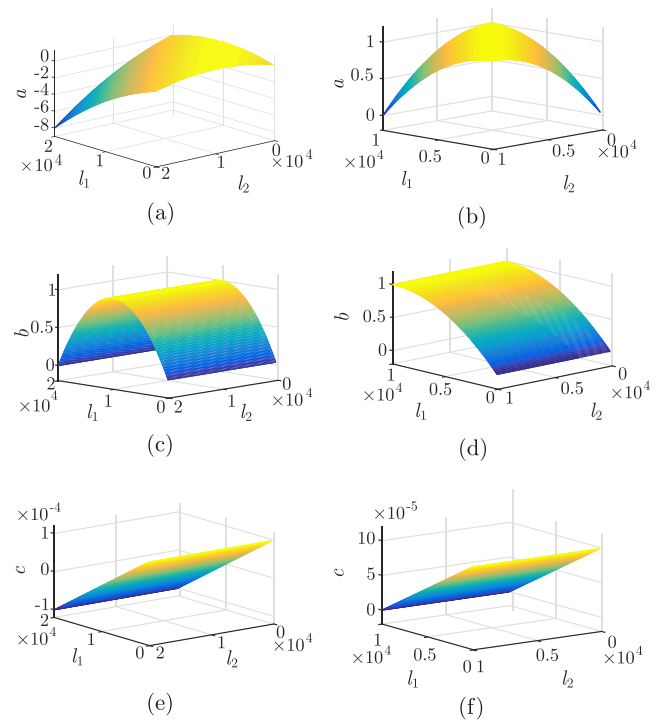


FIGURE 4 Analysis of coefficients a , b and c of (15) with respect to change in the values for gains l_1 and l_2 . (a) Coefficient a in the range of $]0, 2F_s]$; (b) Coefficient a in the range of $]0, F_s]$; (c) Coefficient b in the range of $]0, 2F_s]$; (d) Coefficient b in the range of $]0, F_s]$; (e) Coefficient c in the range of $]0, 2F_s]$; (f) Coefficient c in the range of $]0, F_s]$.

4.1 | Gain design procedure

The choice of controller gains is crucial to obtain high performance of the PMSM drive. High control gain values increase the oscillations of the stator currents, while low gain values can impair the performance of the controller and do not ensure the existence of the sliding surface. From Equations (10), (11) and (15) it is possible to design l_1 and l_2 aiming to obtain an asymptotically stable system. The following conditions must be ensured: $l_2 < 1/T_s$ and $(l_1 + l_2) < 1/T_s$. Thus, the upper bound of the interval can be set to $1/T_s$, which is the switching frequency (F_s).

The impact of the design of the gains l_1 and l_2 in the system stability in accordance with the Lyapunov analysis presented in (15) is demonstrated in Figure 4. The values of l_1 and l_2 are tested as greater than the upper bound (F_s) in Figure 4(a),(c),(e). It is possible to observe that the coefficients a , b and c assume negative values in some regions, as a result, the stability of the system cannot be ensured. Figure 4(b),(d),(f) presents the coefficients a , b and c when the gains l_1 and l_2 are properly designed, $l_1 \in]0, F_s[$ and $l_2 \in]0, F_s[$. In these results, it is observed that the coefficients a , b and c assume only positive values, therefore, the system stability can be ensured such as presented in (15).

The disturbance observer error, expression (11), is implemented in order to analyse the convergence and an appropriated combination of gains for the disturbance observer. Figure 5 presents the disturbance observer error response for three

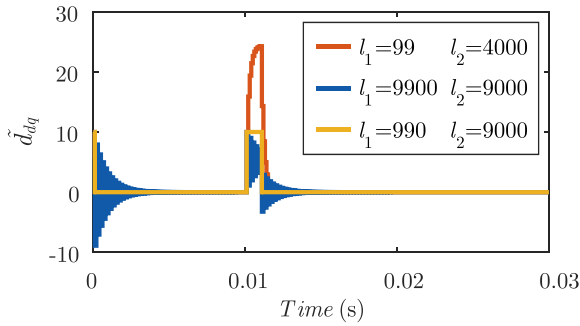


FIGURE 5 Analysis of the design of gains l_1 and l_2 applied to (11)

design combinations of the gains l_1 and l_2 . The system has a positive value for the initial condition ($\hat{\mathbf{d}}_{dq(0)} \neq 0$) and a perturbation is carried out at time 0.01 s ($\Delta \mathbf{d}_{dq(k)} \neq 0$). The first design gives $l_1 + l_2 < 0.5F_s$, as a result, the system response is damped. However, this response presents a slow dynamic. In the second combination, $l_1 + l_2 < 2F_s$, the system response is undamped. The third combination uses $l_1 + l_2 < F_s$. In this case, the system response is damped and it presents a good dynamic response. From appropriate choice of gains, the dynamic of expression (11) tends to zero, even if the system suffers some perturbation, in a short period of time.

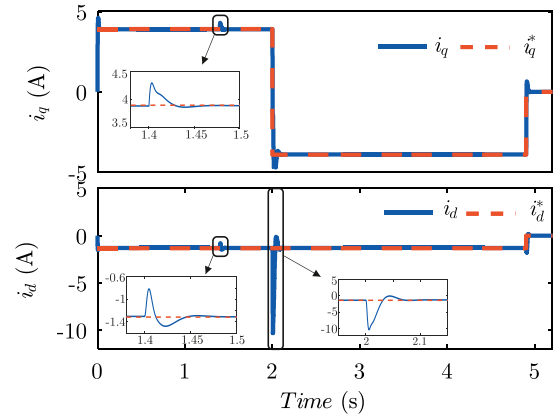
According to the information presented, l_1 and l_2 gains can be designed as follows:

1. Define the upper bound to $(l_1 + l_2)$, by analysing (10), (11) and (15), which ensures that the system is asymptotically stable;
2. Define the expected dynamic system response. A fast dynamic response requires the $(l_1 + l_2)$ near to the upper bound, while for a slower dynamic response, $(l_1 + l_2)$ is adopted significantly less than the upper bound;
3. The current error in (6) is directly related to the l_2 gain. Therefore, to minimise this error, gain l_2 must be set higher than gain l_1 .

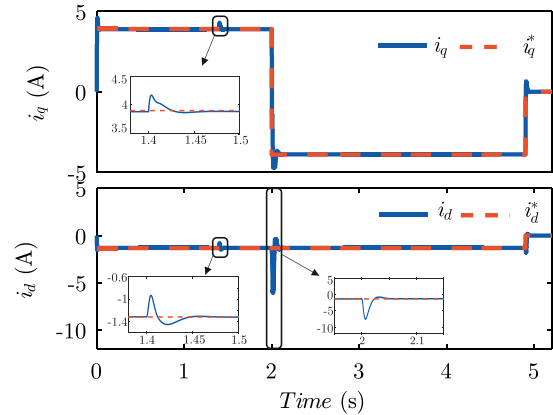
Here, in accordance with the three points, the gain values chosen are $l_1 = 990$ and $l_2 = 9000$.

In [25] the controller gains ϵ and q are defined as, $\epsilon > 0$, $q > 0$ and $(1 - qT_s) > 0$. Alternatively, the approaches in [27] and [28] can be used for the design of the controller gains. Thus, following these guidelines, it was defined here $\epsilon = 450$ and $q = 2750$.

PI and SM controllers were designed aiming to compare the proposed control scheme with conventional methods given in the literature. For the PI design, the first step is the determination of the transfer function that defines the closed-loop dynamics of the stator currents. Besides, it is necessary to define the cutoff frequency and the damping coefficient for the calculation of the proportional and integral gains. The discretisation is based on [47]. The cutoff frequency was defined one decade above the highest natural frequency of the system. The damping coefficient was defined as 0.8, that is, an underdamped condition in order to avoid overshoot in the sys-



(a)



(b)

FIGURE 6 Simulation results of the stator currents with PI and PIDOB controllers implemented in the current control loops. (a) PI controller without decoupling; (b) PI controller with Disturbance Observer (PIDOB).

tem response. The proportional and integral gains obtained for discrete-time implementation of the current PI controllers were respectively, $k_{p_d} = 7.4378$ and $k_{i_d} = 0.1244$ for the d-axis and $k_{p_q} = 15.6521$ and $k_{i_q} = 0.2531$ for the q-axis.

The conventional SMC implemented is based on the control law developed in (26). However, in this case, the PMSM coupling terms, $d_{dq(k)}$, are not replaced by the observed values, $\hat{d}_{dq(k)}$. Therefore, control gains must be redesigned. As the SM control law is based on the plant model, the controller is insensitive to matched uncertainties, but sensitive to mismatched uncertainties. For this reason, the new gains must be greater to compensate the mismatched uncertainties. Thus, it was defined $\epsilon = 2500$ and $q = 9900$.

4.2 | Simulation results

In order to verify the performance of the system under parametric variations, at time of 1.4 s the permanent magnet flux linkage is reduced to 80% of its rated value in all of the simulation results. This parametric variation is adopted in accordance to [1]. Figures 6 and 7 present the simulation results using PI and conventional SM controllers.

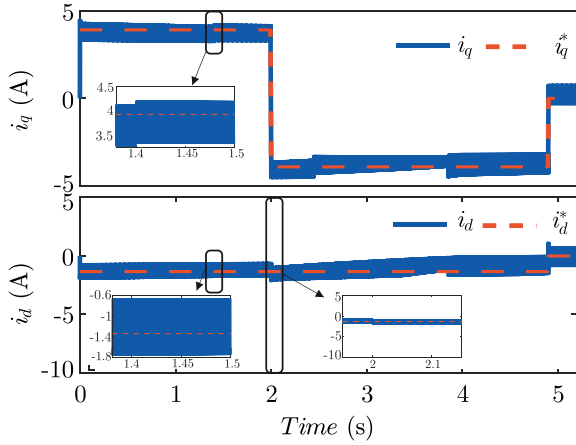


FIGURE 7 Simulation results of the stator currents with a SMC without DO implemented in the current control loops

Figure 6(a) shows the simulation results when a PI controller without decoupling action is used in the current control loop. It is possible to observe the coupling between the axes and the influence of the i_q current variation in the i_d current dynamic. At high rotor speeds the i_d current has more pronounced variations, approximately 10 A, as shown in detail of Figure 6(a) at instant 2 s. Figure 6(b) shows the simulation results when a PI controller is associated to the disturbance observer (PIDOB). These results show smaller oscillations, however, there is still coupling between the axes, a variation of approximately 5.4 A, seen in the zoom of the Figure 6(b) at instant 2 s. It is possible to verify a perturbation in the system response due to parametric variation, in the detail of Figure 6(a), (b) at time of 1.4 s, when the flux linkage is changed.

The simulation results using conventional SMC is shown in Figure 7. The effect of the parametric variation, at the time of 1.4 s, and the coupling between the axes, at instant 2 s, are mitigated with the non-linear controller. However, the chattering in $i_{dq(k)}$ currents presents an amplitude of approximately 1.2 A around the reference. Chattering is a harmful phenomenon, as it, given it decreases the control precision, increases the wear of mechanical components of the machine and heat losses in power circuits [48].

Figures 8 and 9 present the results using the proposed SMC-DOB scheme in the current control loops. The i_d^* and i_q^* current references are the same used in the previous simulation, with PI and conventional SM controllers. Figure 8 presents references for i_d and i_q currents and its simulated values. When the proposed controller is used, the coupling between the dq axes is mitigated even at high rotor speeds, according to the detail in 2 s of Figure 8.

Figure 9(a) presents a comparison between the measured and observed currents and Figure 9(b) shows a comparison between the actual and observed disturbances. The actual disturbances (d_d and d_q) are obtained from the expression (3) and the observed disturbances (\hat{d}_d and \hat{d}_q) in accordance with Equation (6). It is possible to observe the good estimation of the disturbances and currents even with parametric change. The dis-

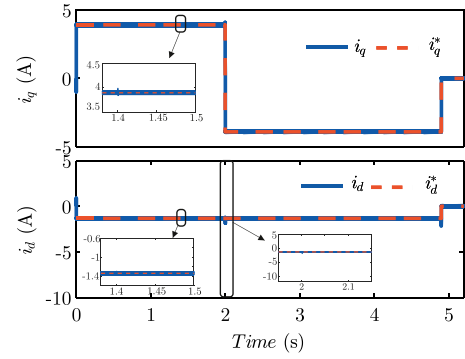


FIGURE 8 Simulation results of the stator currents with SMDOB implemented in the current control loops

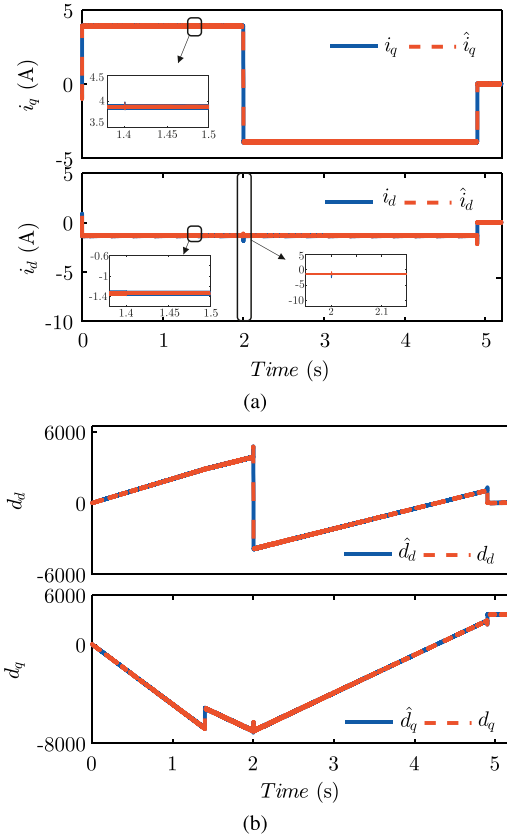


FIGURE 9 Simulation results with the discrete-time SMDOB implemented in the current control loops. (a) i_d and i_q currents, \hat{i}_d and \hat{i}_q observed currents; (b) \hat{d}_d and \hat{d}_q observed disturbance and d_d and d_q actual disturbances.

turbance of the q axis is changed at time of 1.4 S when the flux linkage is reduced and the observed disturbance tracked this variation. It is possible to see by means of the tracking, that the perturbation due to the parametric variation was mitigated, as can be seen in the detail of Figure 8 at the instant 1.4 s.

Simulation results are carried out using the pair of expressions (21) and (26) to illustrate the difference between the systems with and without the inclusion of the digital implementation delay. Note that, when (21) is used, as presented in Figure 11(a), the zigzag motion is not achieved and the system will

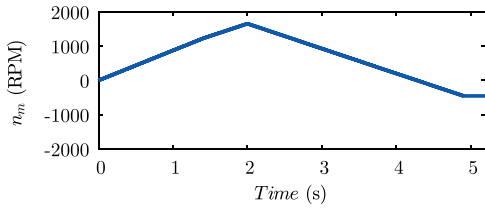


FIGURE 10 Simulation result of the rotor speed behaviour for both implemented current control methods

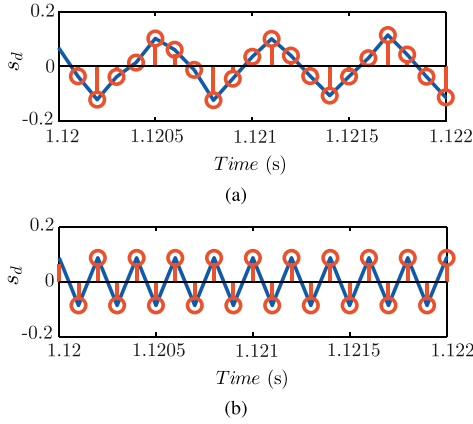


FIGURE 11 Detail of the simulation result of the d -axis sliding surface with the control laws (21) and (26) implemented. (a) Control law implemented by (21); (b) Control law implemented by (26).

not cross the sliding surface at each sampling time. Figure 11(b) gives the switching function when (26) is used as the control law. The system crosses the sliding surface at each sampling period in accordance with the theoretical development. These results demonstrate the importance of the inclusion of the digital implementation delay in the PMSM model. Figure 12 details the change in the reference for the i_q current. It is possible to observe that the i_q current starts to track its reference with a delay of $2T_s$ such as was demonstrated in the theoretical development (see (28)).

4.3 | Experimental results

Figures 13 and 14 present the experimental results when PI and conventional SM controllers are used. The i_d and i_q currents and their respective i_d^* and i_q^* references are shown. The refer-

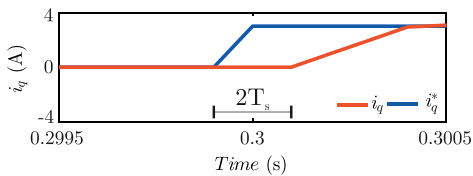


FIGURE 12 Detail of the simulation result: i_q tracking i_q^* with two delays ($2T_s$)

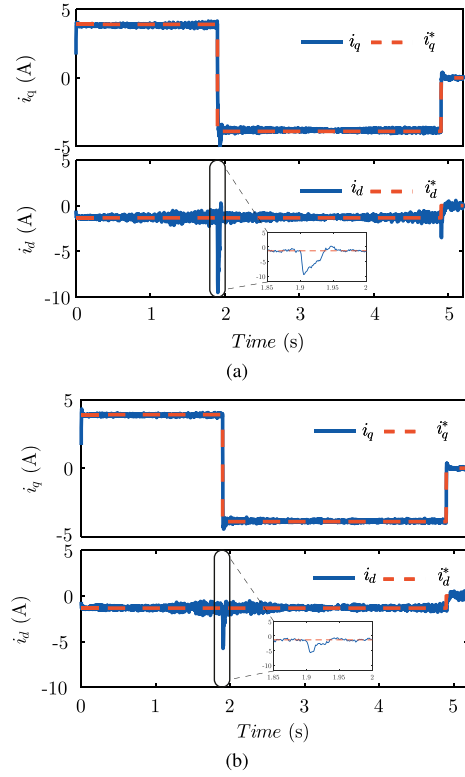


FIGURE 13 Experimental results of the stator currents with PI and PIDOB controllers implemented in the current control loops. (a) Discrete-time PI controller; (b) Discrete-time PIDOB controller.

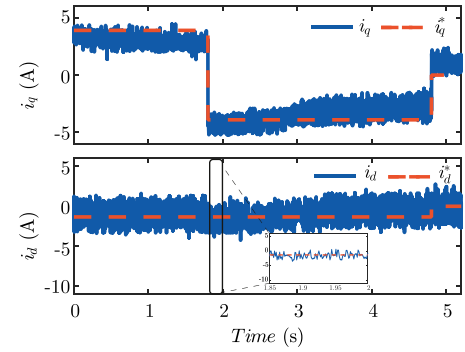


FIGURE 14 Experimental results of the stator currents with the conventional SMC implemented in the current control loops

ence currents are the same used in the simulation results, i_d^* is implemented by (30) while i_q^* is changed.

The experimental result with PI controller without DOB is presented in Figure 13(a). Both currents track their references, however, when i_q is changed a perturbation in i_d is observed. This perturbation is due to the coupling between the axes and it has a direct relationship to the rotor speed value. Figure 13(b) shows the results when a PI controller with DOB is used in the current control loop. The observed disturbance was used as a feed-forward action. The coupling between the axes was reduced, however, it was not totally eliminated. The results using the conventional SMC are shown in Figure 14. The

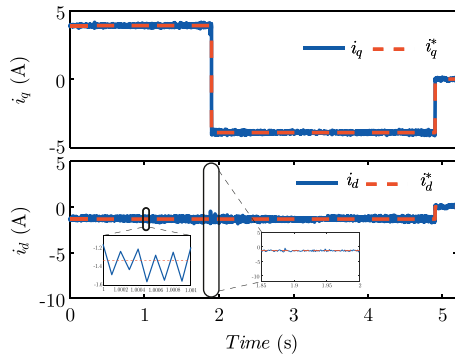


FIGURE 15 Experimental results of the stator currents with the SMCDOB implemented in the current control loops

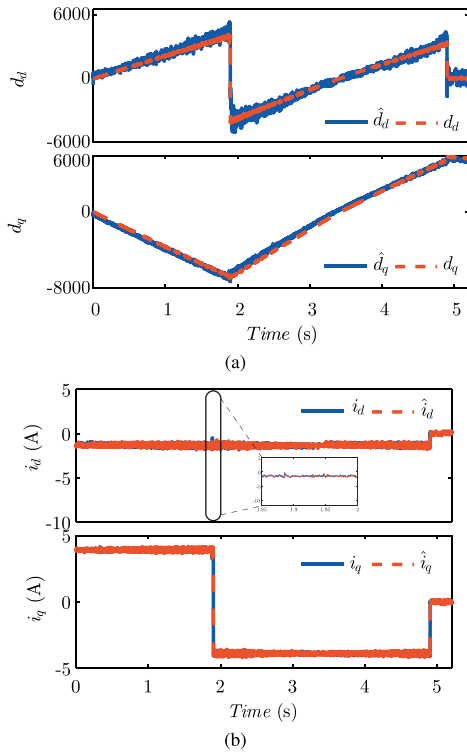


FIGURE 16 Experimental results of the proposed SMCDOB method. (a) Calculated disturbances (d_d and d_q) and estimated disturbances (\hat{d}_d and \hat{d}_q); (b) i_d and i_q currents and \hat{i}_d and \hat{i}_q estimated currents

currents track the references, even when i_q^* is varied at instant of 2 s. However, the high oscillation caused by the chattering, characteristic of the conventional SMC with high gains, can be observed.

Figures 15 and 16 are obtained aiming to evaluate the performance of the proposed discrete-time SMCDOB. Figure 15 presents the i_d and i_q measured currents and the i_d^* and i_q^* reference currents. The proposed current controller has good tracking capability. A good performance of the proposed controller is achieved once i_q is changed and it did not affect i_d dynamic. Thus, the coupling effect between the axes was mitigated.

Figure 16(a) presents the observed (\hat{d}_d and \hat{d}_q) and calculated (d_d and d_q) disturbances. Expression (3) was calculated in

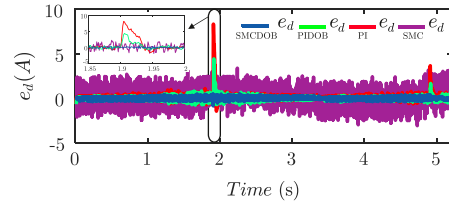


FIGURE 17 Experimental result of the d-axis current error. Comparison of SMCDOB, SMC, PI and PIDOB methods

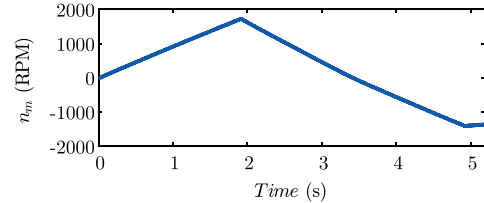


FIGURE 18 Experimental result of the rotor speed behaviour for both implemented current controllers

the software to represent the actual disturbance of the motor. Parametric uncertainties and unmodelled disturbances were neglected in this calculation. The convergence of the estimated disturbance to the calculated disturbance can be observed. Note that the calculated disturbances present a linear characteristic while the observed disturbances present an oscillation around the calculated disturbance. This behaviour is due to the non-ideal characteristic of the motor, that is the back electromotive force and the magnetomotive force present harmonics, there is saturation for some operating conditions. Figure 16(b) gives the \hat{i}_d and \hat{i}_q estimated currents (see (6)). It is possible to observe the good convergence to their measured values.

The d-axis current error, difference between reference and measured current ($e_d = i_d^* - i_d$), are represented in Figure 17. In the zoom of Figure 17, it is possible to observe that when a variation is imposed in i_q the error e_d is closed to zero by using the proposed method and the conventional SMC. However, when using PI and PIDOB controllers this error has a perturbation of approximately 9 and 5 A, respectively. When all results are compared, oscillations in the current using the conventional SMC can be observed. Figure 18 shows the behaviour of the measured rotor speed (open-loop) in both implemented current control schemes. When the i_q current is changed the rotor speed is approximately 1800 RPM, as seen in Figure 18. At high speed the coupling between the current axes is more accentuated, and when the proposed controller is used this coupling is mitigated, in accordance with the comparison presented in the Figure 17.

Figure 19 shows the experimental results with addition of the rotor speed control loop. Thus, i_q^* is generated from the speed error through the proportional-integral compensator. Figure 19(a) shows a step of approximately 100 RPM in the rotor speed reference. Figure 19(b)(top) presents i_q and its reference i_q^* . The i_q current dynamic was similar among the tested current controllers. In Figure 19(b)(bottom), i_d currents and their references are presented. From this result, it is possible

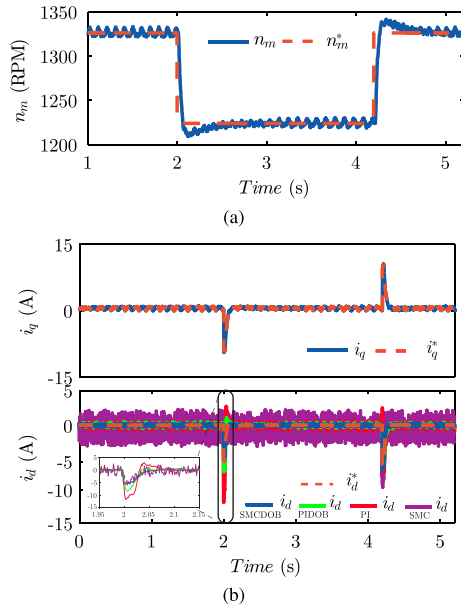


FIGURE 19 Experimental results with a rotor speed reference step using PI, PIDOB, SMC and SMCDOB in the current control loops. (a) Rotor speed behaviour; (b) i_q and its reference, and a comparison among the i_d currents and their references for implemented current controllers

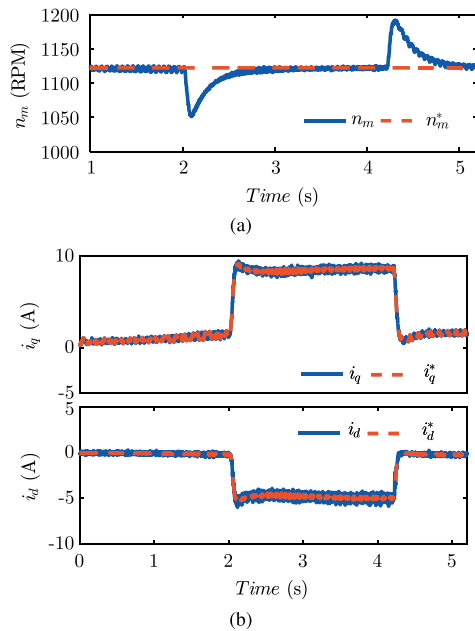


FIGURE 20 Experimental results when a mechanical load is applied using SMCDOB in the current control loops. (a) Rotor speed behaviour; (b) i_d and i_q currents and i_d^* and i_q^* references

to observe that the proposed control scheme presented a better rejection of the disturbance. It is also observed that when the DOB was added to the PI controller, a significant rejection of the perturbation caused by the speed variation was achieved.

The experimental result when a load step is applied to the PMSM is shown in Figure 20. This load step was imposed by means of the IM present in Figure 3. Figure 20(a) shows the behaviour of the rotor speed under effect of the imposed load

disturbance. Figure 20(b) presents the currents and their references. In this test, the good performance of the proposed controller is shown with load condition change.

5 | CONCLUSIONS


This paper has proposed a discrete-time combined control method by means of sliding mode algorithm and disturbance observer aiming to decouple the dq PMSM currents of vector controlled drives. The new proposed disturbance observer is characterised by the presence of an additional state which estimates the stator current of the motor, which improves the convergence of the system and tracks the divergences between the real model and the model used in the control algorithm. The motor model was obtained including the digital implementation delay, which allows the design of a control law suitable to direct implementation in microcontrollers and digital signal processors. Furthermore, it ensured zigzag motion of the discrete-time sliding mode system by means of the modification in the switching functions of the sliding mode control. Stability and convergence analysis were performed in the discrete-time domain. Simulation and experimental results show the effectiveness of the proposed combined control technique. The proposed method can be extended to other application, such as, electrical vehicles, control of grid-tied converters, robotic systems etc.

ACKNOWLEDGMENT

This study was financed in part by the Coordenação de Aperfeiçoamento de Pessoal de Nível Superior – Brasil (CAPES/PROEX) – Finance Code 001, INCT-GD, CNPq (465640/2014-1), CAPES (23038.000776/2017-54) and FAPERGS (17/2551-0000517-1).

ORCID

Thieli Smidt Gabbi  <https://orcid.org/0000-0002-8218-6034>

Hilton Abilio Gründling  <https://orcid.org/0000-0002-7739-2159>

Rodrigo Padilha Vieira  <https://orcid.org/0000-0002-0558-133X>

REFERENCES

1. Krishnan, R.: Permanent Magnet Synchronous and Brushless DC Motor Drives. CRC Press, Boca Raton (2010)
2. Huynh, A., Hsieh, M.F.: Performance analysis of permanent magnet motors for electric vehicles (EV) traction considering driving cycles. *Energies* 11, 1385 (2018)
3. Türker, T., Buyukkeles, U., Bakan, A.F.: A robust predictive current controller for PMSM drives. *IEEE Trans. Ind. Electron.* 63(6), 3906–3914 (2016)
4. Yang, J., et al.: Disturbance/uncertainty estimation and attenuation techniques in pmsm drives—A survey. *IEEE Trans. Ind. Electron.* 64(4), 3273–3285 (2017)
5. Mohamed, Y.A.R.I.: Design and implementation of a robust current-control scheme for a PMSM vector drive with a simple adaptive disturbance observer. *IEEE Trans. Ind. Electron.* 54(4), 1981–1988 (2007)
6. Jung, J.W., et al.: Fuzzy pi-type current controllers for permanent magnet synchronous motors. *IET Electric Power Appl.* 5(1), 143–152 (2011)

7. Zhang, X., Hou, B., Mei, Y.: Deadbeat predictive current control of permanent-magnet synchronous motors with stator current and disturbance observer. *IEEE Trans. Power Electron.* 32(5), 3818–3834 (2017)
8. De Soricellis, M., Da Rù, D., Bolognani, S.: A robust current control based on proportional-integral observers for permanent magnet synchronous machines. *IEEE Trans. Ind. Appl.* 54(2), 1437–1447 (2018)
9. De Soricellis, M., Rapp, H.: Generalised current and voltage shaping method via modified d-q transformation for the torque harmonics correction in PMSMs. *IET Power Electron.* 12(5), 1021–1032 (2019)
10. Gabbi, T.S., et al.: Linear matrix inequalities for digital redesign under delay suitable for PI controllers with application to PMSMs. *Journal of Control, Automation and Electrical Systems*, 30 (2019)
11. Xu, Y., et al.: Robust three-vector-based low-complexity model predictive current control with supertwisting-algorithm-based second-order sliding-mode observer for permanent magnet synchronous motor. *IET Power Electron.* 12(11), 2895–2903 (2019)
12. Wang, Y., et al.: Non-cascade backstepping sliding mode control with three-order extended state observer for PMSM drive. *IET Power Electron.* 13(2), 307–316 (2020)
13. Utkin, V.I.: Sliding mode control design principles and applications to electric drives. *IEEE Trans. Ind. Electron.* 40(1), 23–36 (1993)
14. Utkin, V.I.: Sliding mode control in discrete-time and difference systems. In: Zinober, A.S.I., (ed.) *Variable Structure and Lyapunov Control*, pp. 87–107. Springer, Heidelberg (1994)
15. Corradini, M.L., et al.: A quasi-sliding mode approach for robust control and speed estimation of pm synchronous motors. *IEEE Trans. Ind. Electron.* 59(2), 1096–1104 (2012)
16. Sabanovic, A., Fridman, L., Spurgeon, S.K. (eds.): *Variable structure systems: From principles to implementation*. IET Control Engineering Series, Vol. 66. Institution of Engineering and Technology, London (2004)
17. Zhang, H., Liu, G.: High-performance control method for the MSTMP motor. *IET Power Electron.* 13(2), 266–274 (2020)
18. Zhang, X., Li, Z.: Sliding-mode observer-based mechanical parameter estimation for permanent magnet synchronous motor. *IEEE Trans. Power Electron.* 31(8), 5732–5745 (2016)
19. Corradini, M.L., et al.: Discrete time sliding mode control of robotic manipulators: Development and experimental validation. *Control Eng. Prac.* 20(8), 816–822 (2012)
20. Vieira, R.P., et al.: Discrete-time sliding mode speed observer for sensorless control of induction motor drives. *IET Electric Power Appl.* 6(9), 681–688 (2012)
21. Kali, Y., et al.: Discrete sliding mode control based on exponential reaching law and time delay estimation for an asymmetrical six-phase induction machine drive. *IET Electric Power Appl.* 13(11), 1660–1671 (2019)
22. Dote, Y., Hoft, R.G.: *Microprocessor-Based Sliding Mode Controller for DC Motor Drives*. IEEE IAS Conference Record, pp. 641–645, Cincinnati, USA (1980)
23. Sarpturk, S., et al.: On the stability of discrete-time sliding mode control systems. *IEEE Trans. Autom. Control* 32(10), 930–932 (1987)
24. Furuta, K.: Sliding mode control of a discrete system. *Syst. Control Lett.* (1990)
25. Gao, W., Wang, Y., Homaifa, A.: Discrete-time variable structure control systems. *IEEE Trans. Ind. Electron.* 42(2), 117–122 (1995)
26. Bartoszewicz, A.: Discrete-time quasi-sliding-mode control strategies. *IEEE Trans. Ind. Electron.* 45(4), 633–637 (1998)
27. Bernardes, T., et al.: Discrete-time sliding mode observer for sensorless vector control of permanent magnet synchronous machine. *IEEE Trans. Ind. Electron.* 61(4), 1679–1691 (2014)
28. Silva, G.S., Vieira, R.P., Rech, C.: Discrete-time sliding-mode observer for capacitor voltage control in modular multilevel converters. *IEEE Trans. Ind. Electron.* 65, 876–886 (2018)
29. Li, S., et al.: *Disturbance Observer Based Control: Methods and Applications*. CRC Press, Boca Raton (2014)
30. Chang, J.L.: Dynamic output integral sliding-mode control with disturbance attenuation. *IEEE Trans. Autom. Control* 54(11), 2653–2658 (2009)
31. Repecho, V., Biel, D., Arias, A.: Fixed switching period discrete-time sliding mode current control of a pmsm. *IEEE Trans. Ind. Electron.* 65(3), 2039–2048 (2018)
32. Yang, J., Li, S., Yu, X.: Sliding-mode control for systems with mismatched uncertainties via a disturbance observer. *IEEE Trans. Ind. Electron.* 60(1), 160–169 (2013)
33. Wang, J., et al.: Finite-time disturbance observer based non-singular terminal sliding-mode control for pulse width modulation based DC–DC buck converters with mismatched load disturbances. *IET Power Electron.* 9(9), 1995–2002 (2016)
34. Aksu, I.O., Coban, R.: Sliding mode PI control with backstepping approach for MIMO nonlinear cross-coupled tank systems. *Int. J. Robust Nonlinear Control* 29(6), 1854–1871 (2019)
35. Chen, W.H.: Disturbance observer based control for nonlinear systems. *IEEE/ASME Trans. Mechatron.* 9(4), 706–710 (2004)
36. Chen, W.H., et al.: Disturbance-Observer-Based Control and Related Methods - An Overview. *IEEE Trans. Ind. Electron.* 63(2), 1083–1095 (2016)
37. Yang, J., Chen, W.H., Li, S.: Non-linear disturbance observer-based robust control for systems with mismatched disturbances/uncertainties. *IET Control Theory Appl.* 5(18), 2053–2062 (2011)
38. Zhang, X., et al.: Nonlinear speed control for PMSM system using sliding-mode control and disturbance compensation techniques. *IEEE Trans. Power Electron.* 28(3), 1358–1365 (2013)
39. Gabbi, T.S., Gründling, H.A., Vieira, R.P.: Sliding mode current control based on disturbance observer applied to permanent magnet synchronous motor. In: *Proceedings of 2015 IEEE 13th Brazilian Power Electronics Conference and 1st Southern Power Electronics Conference (COBEP/SPEC) Fortaleza, Brazil* (2015)
40. Yu, L., et al.: Discrete-time sliding-mode switching control scheme with disturbance observer and its application to superheated steam temperature systems. *J. Dynamic Sys., Meas., Control*, 138, 101003 (2016)
41. Qian, R., Luo, M., Sun, P.: Improved nonlinear sliding mode control based on load disturbance observer for permanent magnet synchronous motor servo system. *Adv. Mechanical Eng.* 8(4), (2016)
42. Hao, S., Hu, L., Liu, P.: Sliding mode control for a surgical teleoperation system via a disturbance observer. *IEEE Access* 7, 43383–43393 (2019)
43. Sharma, N.K., Janardhanan, S.: Discrete-time higher-order sliding mode control of systems with unmatched uncertainty. *Int. J. Robust Nonlinear Control* 29(1), 135–152 (2019)
44. Niu, Y., Ho, D.W.C., Wang, Z.: Improved sliding mode control for discrete-time systems via reaching law. *IET Control Theory Appl.* 4(11), 2245–2251 (2010)
45. Ryan, M.J., Lorenz, R.D., Doncker, R.D.: Modeling of multileg sine-wave inverters: a geometric approach. *IEEE Trans. Ind. Electron.* 46(6), 1183–1191 (1999)
46. Morimoto, S., Sanada, M., Takeda, Y.: Wide-speed operation of interior permanent magnet synchronous motors with high-performance current regulator. *IEEE Trans. Ind. Appl.* 30(4), 920–926 (1994)
47. Ogata, K.: *Discrete-time Control Systems*, 2nd ed. Prentice-Hall, Englewood Cliffs (1995)
48. Utkin, V., Lee, H.: Chattering problem in sliding mode control systems. Paper presented at the International Workshop on Variable Structure Systems, Alghero, Italy, 5–7 June 2006

How to cite this article: Gabbi TS, Gründling HA, Vieira RP. Discrete-time sliding mode control based on disturbance observer applied to current control of permanent magnet synchronous motor. *IET Power Electron.* 2021;14:875–887.
<https://doi.org/10.1049/pel2.12071>